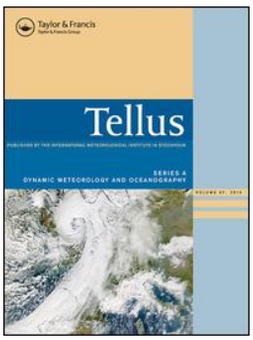

Tellus A: Dynamic Meteorology and Oceanography

ISSN: (Print) 1600-0870 (Online) Journal homepage: http://www.tandfonline.com/loi/zela20

A new climatology of favourable conditions for reverse-shear polar lows

Erik W. Kolstad

To cite this article: Erik W. Kolstad (2006) A new climatology of favourable conditions for reverse-shear polar lows, Tellus A: Dynamic Meteorology and Oceanography, 58:3, 344-354, DOI: 10.1111/j.1600-0870.2006.00171.x

To link to this article: https://doi.org/10.1111/j.1600-0870.2006.00171.x

Tellus (2006), 58A, 344–354
Printed in Singapore. All rights reserved

TELLUS

A new climatology of favourable conditions for reverse-shear polar lows

By ERIK W. KOLSTAD, *Bjerknes Centre for Climate Research, Allégaten 70, 5007 Bergen, Norway*

(Manuscript received 2 May 2005; in final form 23 October 2005)

ABSTRACT

A new climatology of conditions that are favourable for development of polar lows in reverse-shear flow is presented. In such flow, the wind at the low-level steering level is in the opposite direction of the thermal wind in the adjoining layers. A framework for identifying such conditions along with weak lower-level static stability from any gridded data is developed by defining simple dynamical constraints on standard atmospheric fields, applied here to 40 yr of ERA-40 data. The relevance of the constraints is directly demonstrated using satellite images. There are several areas where such conditions occur with high frequency: the Norwegian Sea (>15% of the time during NDJFM), the region to the south of the Denmark Strait (>10%) and the Bering Sea and the Sea of Okhotsk (>5%). In the Nordic Seas region, the polar low season is longer than in the Pacific because the air temperature stays low throughout March. There are primary peaks in December and January and a secondary peak in March, preceded by a distinct nadir in February. A link between the NAO and reverse-shear conditions is suggested.

1. Introduction

Polar lows are intense mesoscale low-pressure systems, usually generated by outbreaks of cold, dry polar air over warm water masses. There is a range of conditions leading to such developments, sometimes referred to as the 'polar low spectrum' (Rasmussen and Turner, 2003). An important group of polar lows are the reverse-shear systems. In contrast to the classical baroclinic systems described by the two-layer omega equation (e.g. Holton, 2004 or Bluestein, 1992a), the conditions are such that the wind at the low-level steering level is antiparallel to the thermal wind in the adjoining layers (Duncan, 1978). The wind speed generally decreases with height and there is a forward tilt of the disturbances in the vertical direction (Rasmussen and Turner, 2003). Typical examples of such conditions occur in positive phases of the North Atlantic Oscillation (NAO), when warm synoptic-scale storms enter the Norwegian Sea from the south (e.g. Rogers, 1997). If the cold fronts of such systems are connected to the inversion over the ice, dry polar air will be pulled southwards, lowering the static stability in the region (e.g. Wu et al., 2004). This has a significant effect on the mesoscale development in the area (Harold et al., 1999).

While reverse-shear conditions are generally considered to be important for a large portion of polar lows to develop, few attemptshave been made to quantify how often, and indeed where and when, such conditions occur. An attempt at such quantifications is made in this paper. However, due to their small spatial and temporal scales, polar lows are difficult to track objectively. Because of this, certain simple dynamical constraints are defined here to identify 'favourable' synoptic conditions for reverse-shear polar low development in the ERA-40 reanalysis data set. The behaviour of these constraints will be validated against a selection of reverse-shear polar lows which have been investigated in other studies.

The main objectives of this study are: (1) to quantify the climatological distribution of such conditions in the current climate, and (2) to provide a framework for identifying such conditions in any data set, e.g. in simulations of future climate scenarios. Accordingly, only basic and widely available atmospheric fields at standard pressure-level surfaces are used in the analysis.

2. Reverse-shear polar lows

Duncan (1977) found that the existence of a vertical wind shear and that the thermal wind and steering-level winds were parallel were necessary conditions for polar lows to develop. Later, he showed that reverse-shear conditions could also be favourable (Duncan, 1978). As mentioned in the introduction, reverse-shear systems differ from the better-known baroclinic disturbances where the growth and movement of the systems are dictated by upper-level troughs. In the classical case, the warm air lies to the right of the background flow, so that the thermal wind is parallel to that flow. The term *reverse shear* means that the thermal wind is antiparallel to the flow. Now the warm air lies to the left of

Corresponding author.
e-mail: erik.kolstad@bjerknes.uib.no

the prevailing winds. The steering level is generally well below 500 hPa and the wind speed decreases with height. In addition, again in contrast to the classical case, there is a forward tilt of the disturbance in the vertical. Behind the disturbance, there is warm advection and rising motion, while downstream there is cold advection and sinking motion. (Businger and Reed, 1989). In other words, a thermally direct circulation is established and the development gains kinetic energy from the reservoir of available potential energy (Rasmussen and Turner, 2003). Figure 1 attempts to visualize this situation in a schematic manner. Diabatic heating near the surface due to release of sensible and latent heat as a result of the cold advection over warm water may further intensify the development (e.g. Montgomery and Farrell, 1992).

The Norwegian Atlantic Current brings warm, saline water into this region (Orvik and Niiler, 2002), leading to high sea surface temperatures at high latitudes even in mid-winter (Rasmussen and Turner, 2003). In positive phases of the NAO, storms tend to extend into the Norwegian and Barents Seas from the south-west. The proximity of the Arctic ice sheet then frequently leads to low static stability and reverse shear in the northerly flow following the cold fronts of such lows. Harold et al. (1999) found that mesocyclones in the 200–400 and 400–600 km diameter range were significantly correlated with the NAO index. As the index became more positive, the small to midsized mesocyclones were more likely to develop. Furthermore, it was noted that such mesocyclones often develop behind synoptic-scale cyclones. For the reasons stated above, the Norwegian and Barents Seas region is considered the primary region for polar lows (Rasmussen and Turner, 2003), and numerous observational and numerical studies of reverse-shear systems have been focussed in this area.

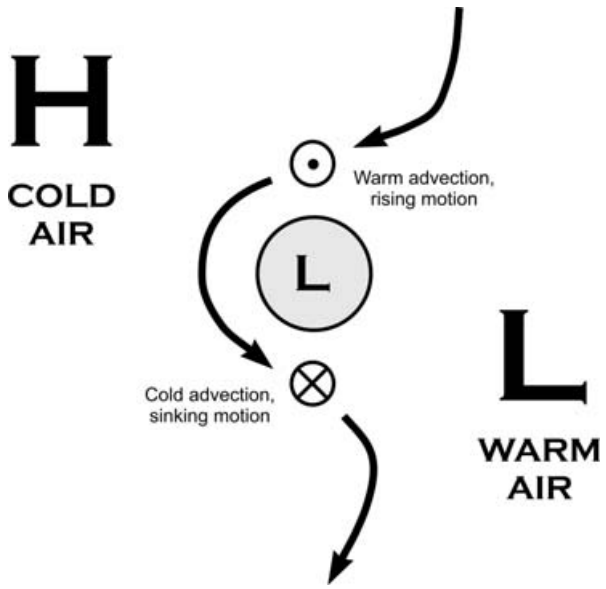

Fig. 1 In this schematic visualization of reverse-shear development, the steering level is seen from above. The synoptic conditions are such that the pressure decreases more or less towards the right of the picture. In other words, the background geostrophic flow has a downward direction. The warm air lies to the right, so the thermal shear is reversed. In the centre of the picture, there is a polar low under development. Advection of warm air and descent upstream of the low, combined with cold advection and descending air downstream ensures a direct thermal circulation. The system thus gains kinetic energy from the reservoir of available potential energy.

A few climatological studies of polar lows in the Norwegian, Greenland and Barents Seas region have been made. In Lystad (1986), the combined results of a study of the periods 1971–82 (Wilhelmsen, 1985) and several studies of the period 1982–85, are presented. The months November-January and March all have frequent polar low sightings. On the other hand, a clear minimum of polar low activity in the region is found in February, but the reasons for this are not discussed in the report. Noer and Ovhed (2003), as an extension of the work presented there, studied the period 1999–2003 using more restrictive criteria. Here, January and March represent distinct maxima of activity, whereas February is still calm. The February nadir is assumed there to be due to a high frequency of 'continental high pressure over Scandinavia', leading to southerly winds in the region. The combined annual cycle of the two studies is displayed in Fig. 2. In terms of spatial distribution, both studies agree that there is a maximum of polar low activity in the region between Svalbard and the northern coast of Norway.

Harold et al. (1999) used satellite images to find 4054 mesoscale cyclones in the North Atlantic over a 2-yr period. For the cyclones with diameters of 200–400 km, the region of maximum winter activity seems to be located along the Norwegian coast, with a secondary maximum just south of the Denmark Strait.

A number of case studies of polar lows have also been performed. Duncan (1978) used atmospheric conditions in the region of a recorded polar low in a simulation, and found that the most unstable wave in his model had a wavelength of 900 km, resembling the observed system.

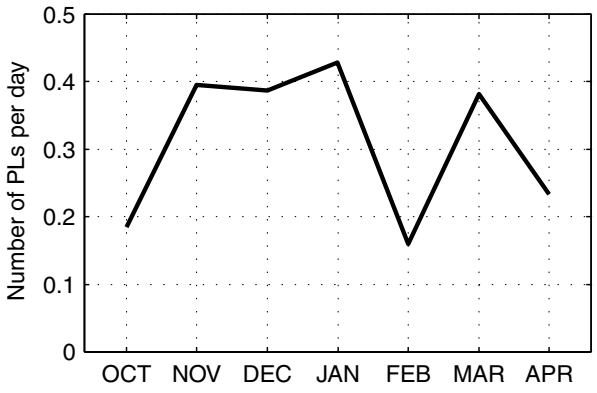

Fig. 2 The total number of polar lows spotted per day in each month in the Norwegian, Greenland and Barents Seas. The study periods were the winters of 1971–85 in Lystad (1986), and 1999–2003 in Noer and Ovhed (2003).

Grønås et al. (1987) used a limited area model to simulate polar lows in the Norwegian Sea, all of them in reverse-shear conditions in northerly flow. The structures were found to be shallow (mainly below 700 hPa) and it was suggested that CISK-like mechanisms intensified the developments.

Four reverse-shear polar lows over the Greenland Sea were studied by Reed and Duncan (1987). The model used by Duncan (1977) was deployed and the fastest growing modes had wavelengths in the 300–1000 km range. The disturbances created by their model were mostly confined to the atmosphere below 700 hPa.

Grønås and Kvamstø (1995) investigated four cases with reverse-shear synoptic conditions favourable for polar lows and found that the height between the tropopause and the convective planetary boundary layer gave a good indication of the possibility for polar low development. In only two of their cases actual polar lows formed, and then that height was 1000 m or less. It was also claimed that northerly winds from an inversion over the ice is a necessary condition for polar low development. Other studies of polar lows in the Nordic Seas region (Nordeng and Rasmussen, 1992; Rasmussen et al., 1992; Claud et al., 2004) will be used to validate the criteria for 'favourable conditions' defined below.

Reverse-shear conditions are not confined to the Nordic Seas. Bond and Shapiro (1991) examined two polar lows in reverse shear over the Gulf of Alaska. Baroclinic instability and release of latent heat was found to represent the main source of eddy kinetic energy in these cases. Mailhot et al. (1996) studied a polar low over the Labrador Sea with strong surface winds and strong low-level baroclinicity in reverse shear. In two studies of a polar low over the Japan Sea (Yanase et al., 2002; Fu et al., 2004), reverse shear is never mentioned explicitly, but it will be seen below that this development took place in such conditions. The two latter developments are also used below to validate the criteria.

3. Definition of criteria

Polar lows are usually confined to the lower levels of the troposphere, so the typical steering level is taken to be at either 775 or 850 hPa. This is consistent with steering-level winds used in simulations based on observational records (e.g. Duncan, 1978). Following Holton (2004), the wind direction at these levels is compared to the direction of the thermal wind in the 700–925 hPa layer, calculated as

$$u_T = -\frac{1}{f}\frac{\Delta(\phi_{700} - \phi_{925})}{\Delta y}, \quad v_T = \frac{1}{f}\frac{\Delta(\phi_{700} - \phi_{925})}{\Delta x}.$$

The two possible angles $\alpha_{1,2}$ between these winds is then given by

$$\cos\alpha_{1,2} = \frac{\mathbf{v}_T \cdot \mathbf{v}_{S_{1,2}}}{|\mathbf{v}_T||\mathbf{v}_{S_{1,2}}|},$$

where $\mathbf{v}_{S_{1,2}}$ is the wind at either 775 or 850 hPa. The first criterion for 'favourable conditions' used here is that at least one of these angles is close to 180°, corresponding to a reverse thermal shear with respect to one of the two candidate steering levels. From a qualitative examination of cloud structures in satellite images, it seems that an angle of no more than 45° from the antiparallel between the thermal wind and the wind at the steering level is sufficient to favour baroclinic development.

As well as reverse thermal shear, low static stability in the lower atmosphere and advection of cyclonic vorticity aloft are considered crucial for polar lows to develop (e.g. Rasmussen and Turner, 2003). It is known from considerations of potential vorticity and thermal wind balance that these two features are closely correlated (Bluestein, 1992b). With this relationship in mind, one can consider the stability in the lower levels, e.g. up to the 700-hPa surface, a tracer of upper-level disturbances. The Rossby radius of deformation is defined in Holton (2004) as

$$L_R \equiv NH/f_0,$$

where f_0 is the Coriolis parameter, H is the height of the tropopause and N is the Brunt-Väisällä frequency. Small values of N allow upper-level disturbances to penetrate greater vertical distances and even small-scale disturbances aloft are able to reach far down towards the surface. To assess the lower-level static stability, a dimensionless normalized radius of deformation defined as

$$R_N \equiv L_R/H = N/f_0$$

is used. N is calculated in the 700–925 hPa layer as the real part of

$$N = \sqrt{g\frac{\Delta(\ln\theta)}{\Delta z}}.$$

The second criterion for favourable polar low conditions is that R_N must be small. Using one discrete boundary is somewhat arbitrary. However, deciding against splitting the analysis in two or more parts, using different thresholds for R_N, 80 is taken as the upper boundary. This is based on an empirical trial and error procedure, using satellite images as a qualitative reference. Also, using $H = 5$ km then yields an upper boundary of 400 km for L_R, which is within the mesoscale domain.

Six-hourly atmospheric data from the ERA-40 gridded reanalysis project for the polar low season from October to April from 1960–61 to 1999–2000 are used in the analysis. The horizontal resolution of the data is 2.5° by 2.5°, corresponding to a distance of 280 km in the zonal direction between the grid points at the equator and half of that at 60°N. The smoother coarse-resolution interpolated version of the ERA-40 data was chosen instead of the original one with higher horizontal resolution (1.125° by 1.125°), because the latter version includes mesoscale features. Since the intent here is to look at synoptic 'background' conditions, this would to some extent represent noise in the data. For each 6-hourly set of values, the parameters are calculated for each grid point from 40°N and northwards. When both the criteria, i.e. $135° \leq \alpha_{1,2} \leq 225°$ and $R_N \leq 80$, are fulfilled, the location and time of the polar low *potential* are recorded. To quantify the annual cycle inside selected regions, the percentage

of the total number of grid points with such potential in each region was calculated.

An approach such as this, using rigid thresholds as constraints on a few selected atmospheric fields, gives a rather crude measure of the probability of polar low development. There will necessarily to be both false positive (type I errors) and false negative selections (type II errors). For instance, baroclinicity does not explicitly take part in the selection process, so shallow, low-level fronts are neglected. Similarly, sudden small-scale upper-level forcing in situations with no distinct lower-level instability will also be overlooked. Those are both examples of potential false negative selections. In other cases, the synoptic conditions as far as lower-level stability and direction of the thermal shear may be suitable, but the upper-level forcing needed to trigger the development may be missing. Likewise, since no thresholds are applied to the surface temperature, the stability might be sufficiently low, but the sea surface too cold for substantial development to take place. In such cases, there will be false positive selections (see Section 4.5). Nevertheless, it will be seen in the following section that the criteria correspond quite well overall with actual reverse-shear polar lows.

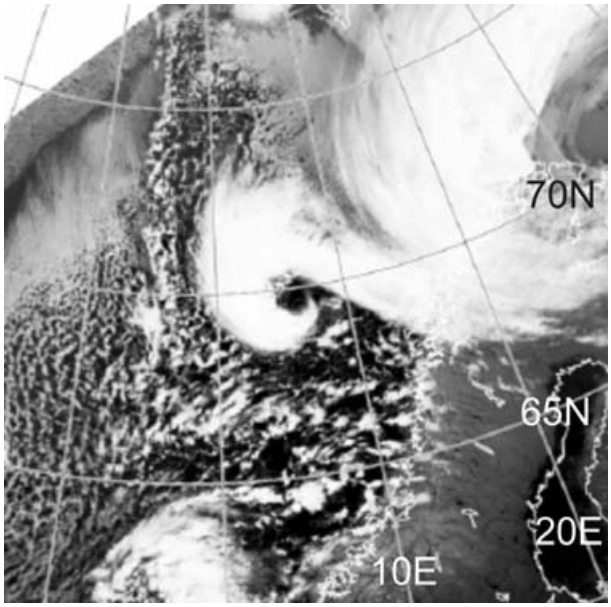

Fig. 3. A satellite image taken of 'le Cygne', taken at 1341 UTC 14 October 1993. The polar low is seen off the western coast of Norway at approximately 70N latitude. Adapted from Claud et al. (2004).

4. Validation of criteria

The above selection of constraints was based on previous studies of the mechanisms leading to reverse-shear polar low development. Here, satellite images are compared to maps of potential polar lows according to the criteria defined above.

4.1. 14–15 October 1993; Norwegian Sea

This polar low development has been studied in great detail in Claud et al. (2004), where it was dubbed 'le Cygne' due to its swan-like appearance. With a lifetime of roughly 72 h, this was an unusually long-lived polar low. In-between a synoptic low (the cloud system seen at 72–73°N, 35°E in Fig. 1 in Claud et al., 2004) passing over Scandinavia from the south-west and a high over Greenland, a large portion of the Norwegian and Barents Seas was characterized by reverse shear and weak static stability in the lower layers. Inside this region, 'le Cygne' formed early on 14 October and moved in a southerly direction until its collapse in the North Sea on 16 October. A satellite image taken at 1341 UCT on 14 October 1993 is included here in Fig. 3. Roll clouds such as the ones seen in this picture are often associated with cold-air outbreaks, large air-sea temperature differences and high surface wind speeds (Liu et al., 2004). Figure 4 is a map illustrating the behaviour of the constraints at approximately the same time. In the unshaded white regions, there is neither reverse shear, nor low static stability. Over the areas with the lightest gray shading, there is reverse shear with reference to one of the two candidate pressure levels defined above, but insufficiently low static stability. The next tone of shading denotes regions with low static stability, but without reverse shear. Finally, the darkest gray shading indicates regions where both criteria are fulfilled simultaneously, thus implying a potential for polar lows. It is clearly seen that the southern part of the whole region displayed in Fig. 4 is characterized by low stability in the lower layers,

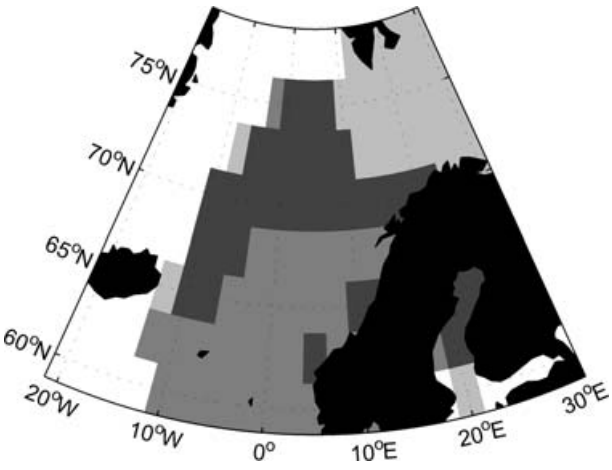

Fig. 4. A map showing the different parameters at 1200 UTC 14 October 1993 in an area similar to the one depicted in Fig. 3. The ERA-40 grid boxes are shaded according to the following legend from white to dark grey: (1) Neither reverse shear at the 850-hPa (black) or the 775-hPa levels, nor is the normalized radius of deformation R_N less than 80. (2) Reverse shear, but not sufficiently low static stability. (3) Low static stability, but not reverse shear. (4) Both reverse shear and low static stability according to the criteria defined in the text. The latter grid boxes, in dark grey shading, define the areas with favourable conditions for reverse-shear polar low development.

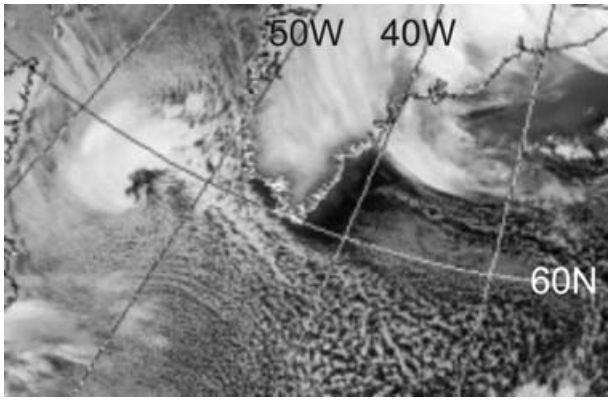

Fig. 5. An image of the polar low discussed in Mailhot et al. (1996), taken at 1509 UTC 11 January 1989. The polar low is situated just west of Cape Farewell (on the southern tip of Greenland) at this time. The image was taken from the Dundee Satellite Receiving Station.

and that there is reverse shear in the northern part. 'Le Cygne' is decidedly inside the region where the two conditions combine.

4.2. 11–12 January 1989; Labrador Sea

This polar low in the Labrador Sea is studied in depth in Mailhot et al. (1996). In Fig. 5, a satellite image taken at 1509 UTC 11 January 1989, the polar low is clearly seen on the left. Figure 6 is a snapshot of the criteria at 1800 UTC on the same day. At the time, a synoptic-scale low was situated to the south-west of Iceland, leading to the northerly winds in reverse-shear flow in the Labrador Sea. Roll clouds are predominantly seen in the region with low static stability. The most darkly shaded region coincides quite well with the observed polar low.

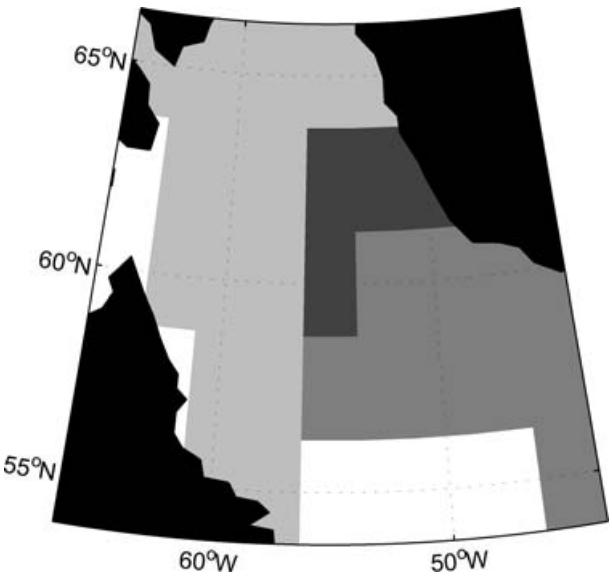

Fig. 6. As in Fig. 4, but now at 1800 UTC 11 January 1989. The area is similar to the one depicted in Fig. 5.

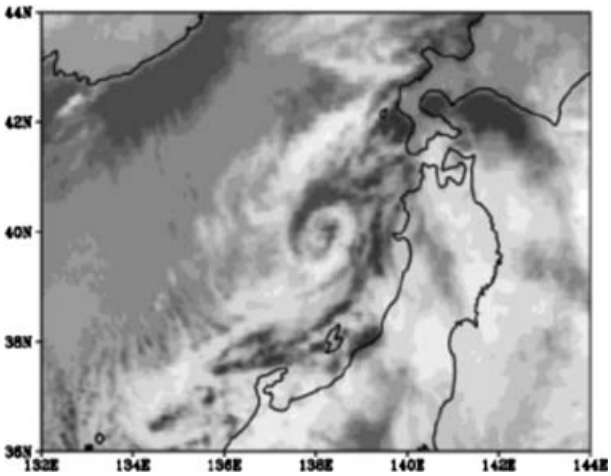

Fig. 7. A reproduction of Fig. 9a in Fu et al. (2004), taken at 1800 UTC on 21 January 1997. This is the Japan Sea with Hokkaido island in the upper right corner.

4.3. 21 January 1997; Japan Sea

A polar low observed in the Japan Sea on 21 January 1997 was investigated by Yanase et al. (2002) and Fu et al. (2004). It formed to the west of Hokkaido island and moved southeastward with a speed of about 40 km h^{-1}. Figure 7 is an image of the cloud-top equivalent blackbody temperature (TBB) estimated from Geostationary Meteorological Satellite-5 infrared data of the Japan Meteorological Agency, taken at 1800 UTC on that day. It is clearly seen that the flow in the area north of the development was from the north or north-east (as mentioned in Fu et al., 2004). No specific mention of reverse shear is made in either paper, but it can be seen from Fig. 8, a representation of the criteria at the same time, that almost the entire area displayed there had reverse

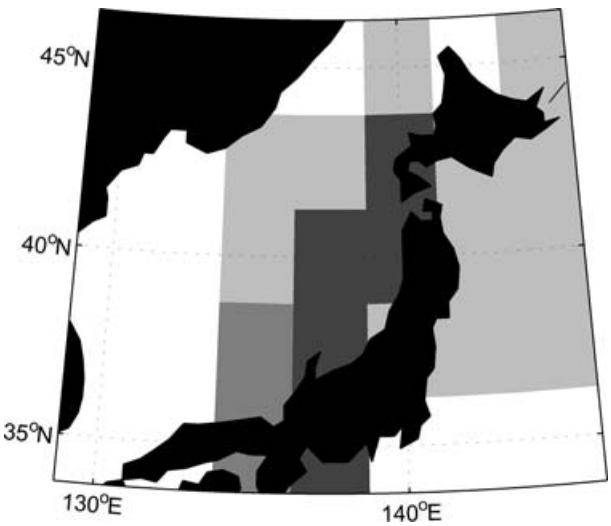

Fig. 8. As in Fig. 4, but now at 1800 UTC 21 January 1997. The area is similar to the one in Fig. 7.

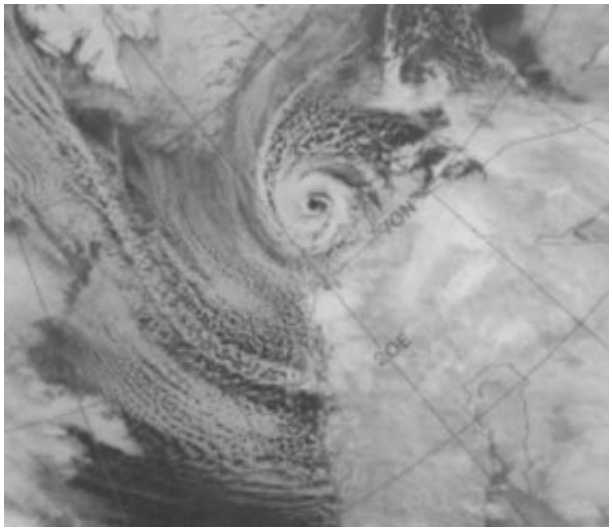

Fig. 9. A satellite image taken on 27 February 1987 of a polar low just north of the northern coast of Norway. The image was taken from http://meted.ucar.edu/norlat/snow/polarlows/.

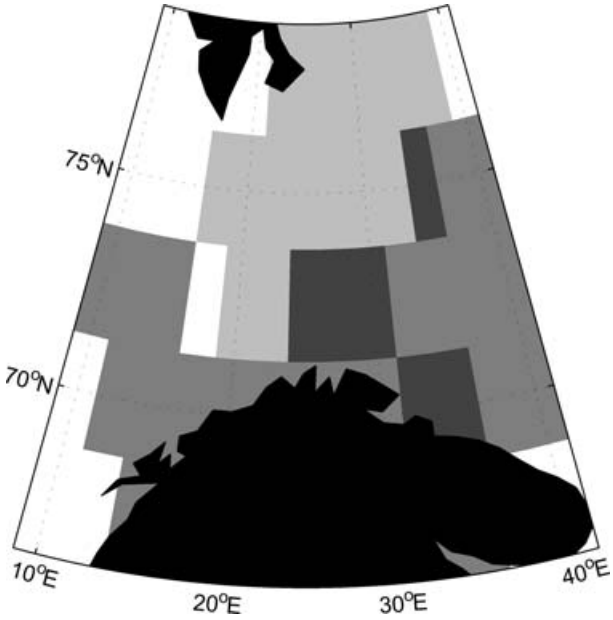

Fig. 10. As in Fig. 4, but now at 0000 UTC 27 February 1987. The area is similar to the one depicted in Fig. 9.

shear. In the most darkly shaded area, there was low stability as well, and this area matches the cloud structures in Fig. 7.

4.4. 26–27 February 1987; Barents Sea

This polar low was studied by Nordeng and Rasmussen (1992). Figure 9 is a satellite image taken at 0418 UTC on 27 February 1987. On the synoptic scale, it is seen from the cloud streets to the north of the polar low that there was a large-scale low to its east, which cloud system can be seen in the image. The passage of this low across the Norwegian Sea led to a northerly flow, reverse shear and weak static stability in a large region. It is also seen that the ice reaches as far south as the 75°N latitude, implying that the baroclinicity in the region must have been substantial in northerly flow regimes. Figure 10 gives an outline of the criteria at 0000 UTC on the same day. The reverse-shear flow due to the synoptic low is seen towards the top of the map, and the actual polar low is inside the region where the stability was low at the same time.

4.5. 15 December 1982; Barents and Norwegian Seas

In the days leading up to the 15 December 1982, there were multiple polar low developments in the Barents Sea (Rasmussen et al., 1992). Despite there being northerly winds and a distinct cold air outbreak over the region, initially the alignment of the isotherms were not such that there was large-scale reverse shear. However, the stability was low in the region, and an upper-level disturbance triggered the polar low dubbed 'A' by Rasmussen et al. (1992) on the 12th. As this low strengthened and deepened, other smaller-scale developments followed and an increasingly larger portion of the area had reverse shear. When a fast-moving synoptic low in full development came in from Iceland towards the Norwegian coast, the two lows 'connected' and altered the flow direction to one quite parallel to the isotherms, and reverse shear dominated the Norwegian Sea region. Figure 11 is a satellite image taken at 0406 UTC on 15 December. In Fig. 12, which displays the criteria at 0600 UTC on the same day, the reverse-shear conditions and the low stability prevailing in the region are

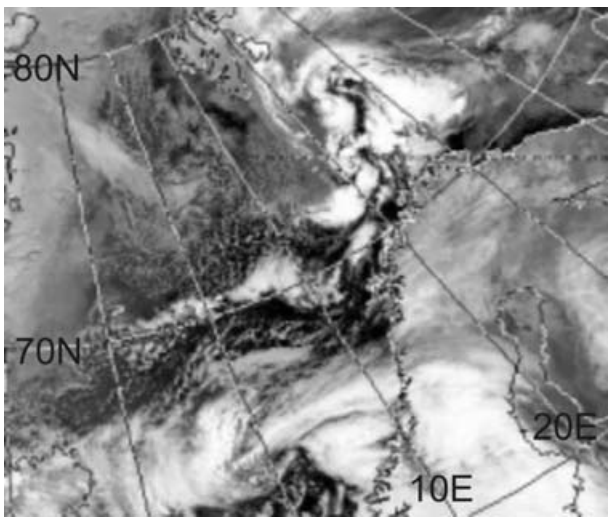

Fig. 11. A satellite image taken at 0406 UTC 15 December 1982, and found at the Dundee Satellite Receiving Station. Near the top of the image, there are several polar lows in different stages of their life cycle. The Scandinavian mainland is seen to the right, and Spitsbergen and Svalbard near the upper left corner.

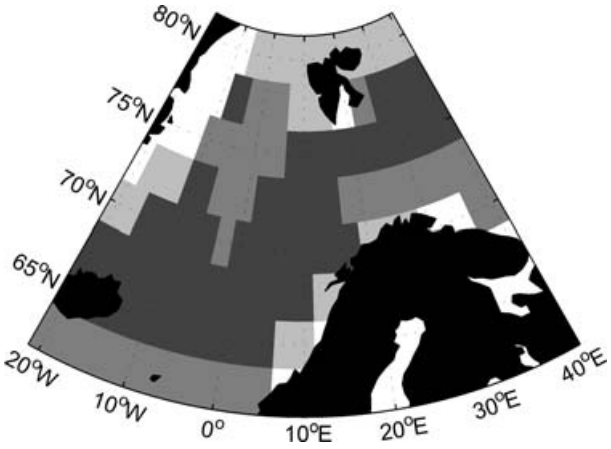

Fig. 12. As in Fig. 4, but now at 0600 UTC 15 December 1982. The area is similar to the one in Fig. 11.

clearly seen. It is also clear that this is an example of the criteria selecting a rather large region, in contrast to the more confined regions selected in the previous examples. There are polar lows, both decaying and developing, in the area between the coast of Norway and Svalbard as discussed by Rasmussen et al. (1992), and these are clearly captured by the criteria. However, no explicit mention of polar lows in the Norwegian Sea is made in that paper. Although it is clear from the cloud structures that there is some small-scale convective development in the region, the larger-scale cloud system east of Iceland belongs to a front associated with the synoptic low moving in from the west. No explicit evidence for polar low development is seen, and this could well be a case of false positive selection. A possible reason for this could be that there were insufficient upper-level disturbances to trigger polar lows.

5. Climatology of favourable conditions

It has now been established that the criteria defined above identify favourable conditions for reverse-shear polar low development. To investigate the climatology of those conditions, the number of cases over 40 seasons with polar low potential are counted.

5.1. Spatial distribution

In Fig. 13, the percentage of the time for each grid point during November to March (NDJFM) from 1960–61 to 1999–2000 with polar low potential is displayed. As expected, there is a distinct maximum of potential in the Norwegian Sea, reaching into the Barents Sea, agreeing with the climatological results of both Lystad (1986) and Noer and Ovhed (2003). The constraints are satisfied roughly 10–15% of the time in that area. The region to the west and south-west of Iceland represents another local maximum of such conditions. The part of the map that covers the North Atlantic is similar to the spatial distribution of 200–400 km wintertime mesocyclones in Harold et al. (1999, their

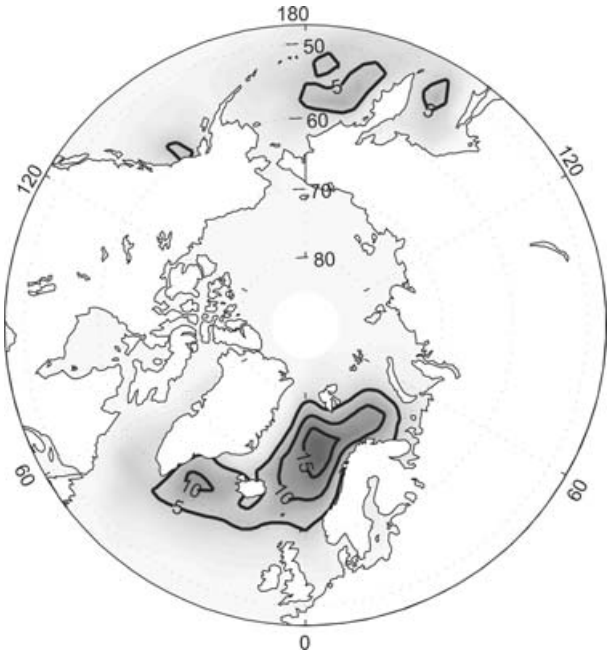

Fig. 13. The mean percentage of the time during NDJFM 1960–61 to 1999–2000 for each grid point with reverse thermal shear and low static stability according to our constraints.

Fig. 2b). However, their maxima in the Denmark Strait and in the Norwegian Sea are both on the order of 2–3% (DJF occupation time). Recalling that the criteria used in this study are not designed to select actual polar lows, this difference in magnitude is perhaps not so surprising. In the North Pacific, the Sea of Okhotsk and the Bering Sea are also quite frequently subject to such conditions.

In terms of reverse thermal shear, Fig. 14 shows the percentage of the total NDJFM period when $135^\circ \leq \alpha_{1,2} \leq 225^\circ$. In the North Atlantic, the most affected regions are those to the west and north-west of the mid-latitude storm tracks, with the warm air to the east, corresponding to a southerly thermal wind. The persistence of the reverse shear in the Denmark Strait is probably due to this region being 'trapped' between the Icelandic low and the Greenland High. However, the Greenland, Norwegian and Barents Seas regions are also prone to such conditions. This can also be said about the Bering Sea and the Sea of Okhotsk. On the whole, it is clear that the regions known for polar low development all have high frequencies of reverse shear.

The percentage of the wintertime when $R_N \leq 80$ is shown in Fig. 15. The stability is generally quite weak in the Norwegian and Barents Seas, where the constraint on R_N is satisfied nearly half the time. The proximity of the ice edge and the large extent of relatively warm open water at high latitudes, combined with a high frequency of northerly winds following the passage of extratropical storms, are the main reasons for this. In the North Pacific, the temperatures near the sea surface are lower compared

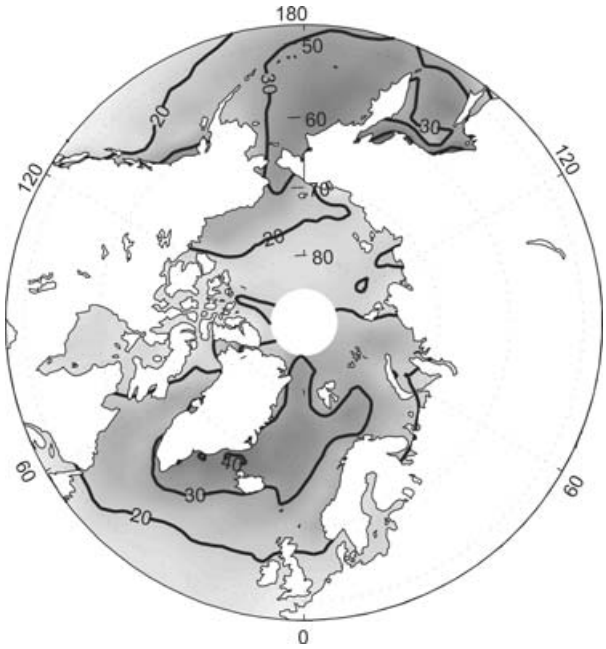

Fig. 14. As in Fig. 13, but now with the reverse-shear constraint only.

to the mid-level ones, so that the high frequencies of unstable air masses found in the North Atlantic are not matched.

5.2. Annual cycle

With regards to the local maxima in Fig. 13, two regions were chosen for further analysis: a sector of the Norwegian Sea (NS

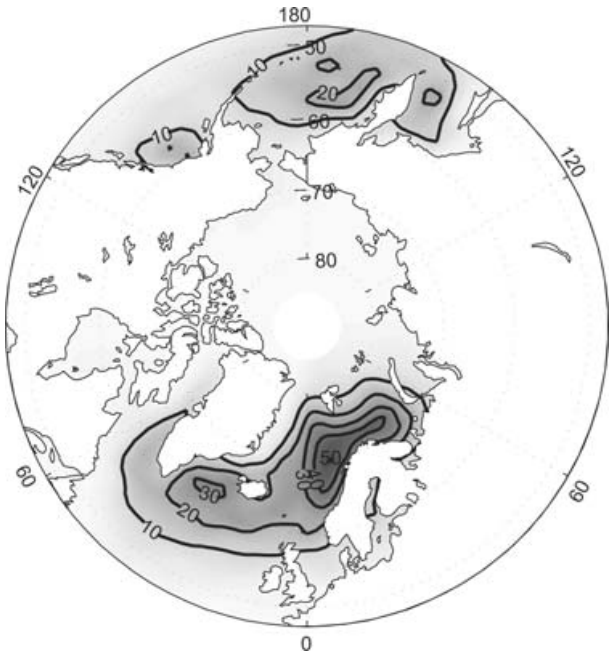

Fig. 15. As in Fig. 13, but now with the low stability constraint only.

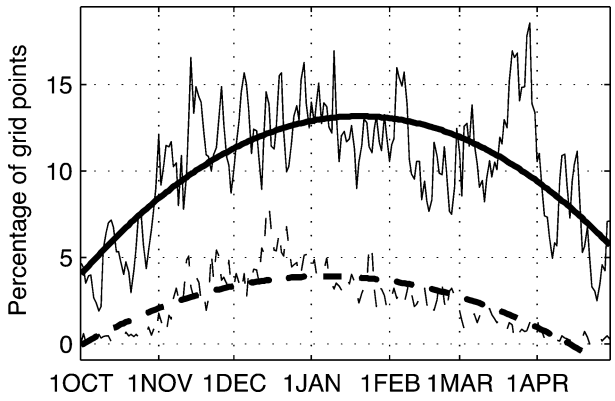

Fig. 16. The temporal distribution of the number of cases with reverse thermal shear and low static stability in two regions: The Norwegian Sea (NS in the text; solid lines) and Sea of Okhotsk (SO; dashed lines). The values are 40-yr averages of daily means of the percentage of the grid points in each region for which the criteria are satisfied for each date from 1 October to 30 April. Quadratic polynomial trends are displayed with thick, black lines and long-term daily mean values with thin, grey lines.

from now on: latitudes from 67.5 to 75 and longitudes from −12.5 to 12.5) and a sector of the Sea of Okhotsk (SO: latitudes from 47.5 to 57.5 and longitudes from 145 to 155). The average percentage (over 40 seasons) of their respective total number of grid points with potential for polar lows every 6 h from 1 October to 30 April is then calculated. As a consequence of the noisy nature of the resulting 'time series', long-term daily means and simple second-order polynomial trends are displayed in Fig. 16. As expected, the winter is the most active polar low season. In both regions, the peak of such activity occurs around new year. In terms of daily means, the local peak in late March in the Norwegian Sea sector stands out. It is obvious that this peak is significant. Similarly, there is a nadir in mid- to late February. This agrees well with February nadirs found by Lystad (1986) and Noer and Ovhed (2003). Although not shown here, the region to the south of the Denmark Strait shows a similar behaviour to

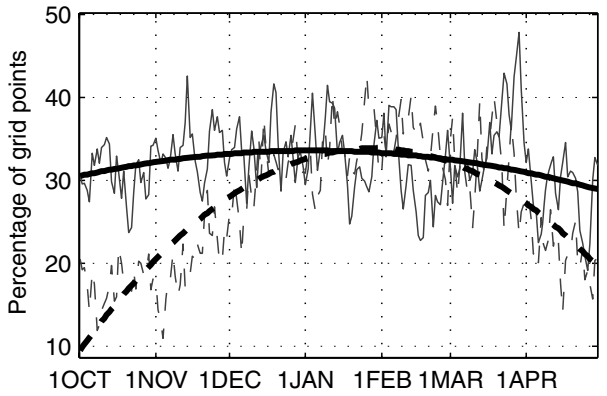

Fig. 17. As in Fig. 16, but now with the reverse-shear constraint only.

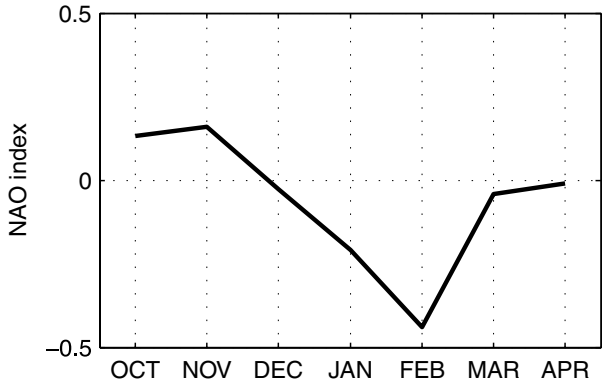

Fig. 18. The mean monthly NAO index from May 1960 to April 2000. The numbers were obtained from the Climate Prediction Center at http://www.cpc.ncep.noaa.gov/.

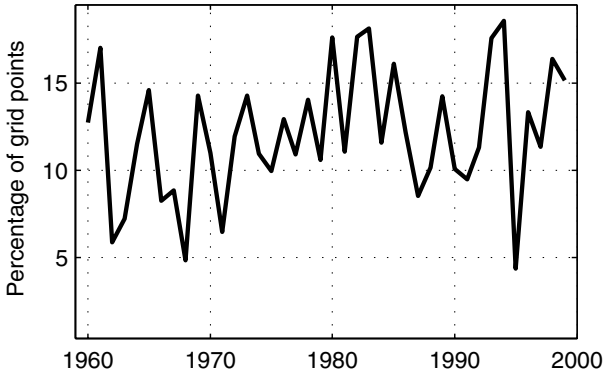

Fig. 20. The interannual variability of occurrences of polar low potential for NS (solid line) and SO (dashed line). The values are the average percentage of grid points in each region with reverse shear and weak static stability for each NDJFM season from 1960–61 to 1999–2000.

that of the Norwegian Sea, but the February nadir and the March peak occur a little earlier in the southernmost region.

The temporal distribution of reverse-shear conditions is displayed in Fig. 17. A peak is found near the end of March in the NS region, corresponding very well with the similar peak in Fig. 16. This strongly suggests that this peak is closely tied to storms passing through the region from the south-west, as these storms are instrumental in generating reverse-shear conditions in this region. As mentioned above, Harold et al. (1999) found the correlation between positive phases of the NAO and small to midsized mesocyclone activity in the Nordic Seas to be significant. The average monthly NAO index from October 1960 to April 2000 is displayed in Fig. 18. It is clear that according to the index, February generally represents a minimum of corresponding synoptic activity, thereby most likely decreasing the number of reverse-shear situations in the Norwegian Sea. This agrees well with the claims made by Noer and Ovhed (2003) that the February minimum is related to a higher frequency of high-pressure systems over Scandinavia in that month. Furthermore, it is noted that there is a sharp increase in the index from February to March, complying with the peaks and nadirs in Figs 16 and 17. However, there is not a one-to-one correspondence between the NAO index and reverse shear. For example, even though the index takes relatively high values in October, there is not an especially high frequency of reverse shear then in the Norwegian Sea compared to in March. This is because the air is much colder in March due to the strong cooling of the polar region throughout the winter. The Arctic ice sheet does not extend far to the south in October. From Kvingedal (2004), it is known that the ice edge normally reaches its southernmost boundary in the beginning of April. The corresponding minimum of ice extent occurs in September. Thus, the mid-level temperatures in October are not especially low, and there will not be as much low-level baroclinicity or instabilities (and reverse shear in northerly flow) as in March, when the temperatures at mid-levels are generally much lower. This can be seen from the temporal distribution of the low stability-constraint (Fig. 19). The temperature stays cold throughout March in the Norwegian Sea. In the Sea of Okhotsk,

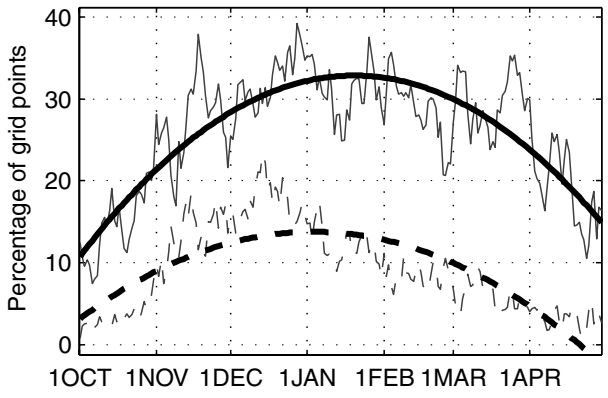

Fig. 19. As in Fig. 16, but now with the low stability constraint only.

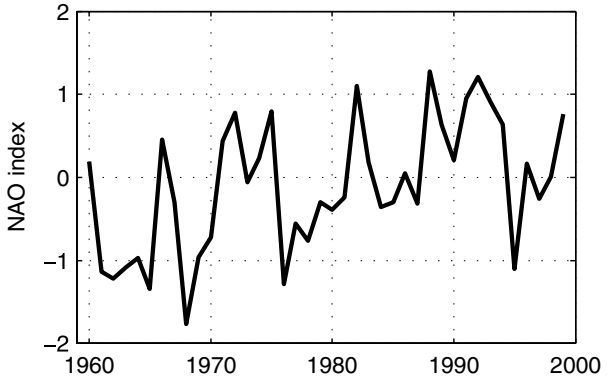

Fig. 21. The yearly mean NDJFM NAO index. The numbers were obtained from the Climate Prediction Center at http://www.cpc.ncep.noaa.gov/.

at lower latitudes, the spring warming takes place earlier, and stability is restored.

The similarities between Figs 17 and 19 might give the impression that the two constraints are correlated. However, this does not seem to be the case. By picking a grid point in the Norwegian Sea, it is found that the frequency of low stability does not increase as the angle between the thermal wind and the flow at 775 or 850 hPa increases towards 180° (not shown).

5.3. Interannual variability

The average percentage of grid points with polar low potential in each region over 40 seasons is displayed in Fig. 20. The standard deviances amount to 3.5% for NS and 0.9% for SO. In other words, there is a fairly large year-to-year variability. It is likely that there is a link between the number of occurrences of potential during one winter and the frequency of blocking high-pressure systems over Scandinavia over the same period. In Fig. 21, the mean yearly NDJFM NAO index is shown. The link to the NAO is clear, but again not one-to-one. In 1968–69 and 1995–96, little polar low potential was recorded in the Norwegian Sea, and these years were also deeply in the negative NAO terrain. On the other hand, 1971–72 also had little potential, but the NAO was positive. Although the approach used here is a crude one, the connection between the NAO, or indeed other teleconnection patterns, and reverse-shear conditions might merit further exploration in the future.

6. Conclusions and future directions

Situations during a 40-yr period that were characterized by reverse thermal shear and low static stability in the lower layers of the atmosphere have been identified in the ERA-40 data. Such conditions are known to be favourable for polar low development. By defining certain constraints representing such conditions using standard atmospheric fields, it is possible to identify them in any gridded data set. To define the constraints, their behaviour was visualized at the time and location of known polar low developments. For simplicity, discrete threshold values were used. A possible future refinement of the method would be to use multiple thresholds when defining the criteria. It could also be interesting to include a criterion for low-level baroclinicity, which is also very important for polar low development (Rasmussen and Turner, 2003). However, in the majority of the situations captured by the constraints, it was seen from satellite images that there were at least indications of polar low development. This suggests that it would be meaningful to look for such conditions when forecasting polar lows. It is also possible to apply the constraints to model simulations of future climate scenarios.

An analysis of the spatial and temporal distribution of these conditions constitute a new climatology of favourable conditions for reverse-shear polar lows. Such conditions occur with relatively high frequency (10–15% of the time) throughout the winter months in the Norwegian Sea, a result which is compatible with earlier climatological studies. Several other local maxima for favourable conditions for polar low development were also found: in the region south of the Denmark Strait (around 10%), in the Bering Sea and in the Sea of Okhotsk (both around 5%). Two key regions were defined for the study of the annual cycle: a sector of the Norwegian Sea and the Sea of Okhotsk. The polar low season in the former region is longer than in the latter. This is mostly because the air temperature stays low for a longer period in the north eastern Atlantic. The sea-ice maximum there normally occurs in the beginning of April. Because of that and the high latitudes of the region, the temperatures stay low in the Nordic Seas throughout March. During the cold winter months, storms coming into the region from the south-west in positive phases of the NAO are thus likely to be followed by reverse-shear conditions and weak static stability. Furthermore, it was found that there is a relatively quiet period with regards to polar low activity in the Norwegian and Barents Seas around February. This lapse is followed by a brief but significant active period in mid- to late March. The annual cycle of the NAO index is at its most negative in February. In March, on the other hand, the average NAO index is considerably higher, indicating that the synoptic storm tracks are more favourable for polar lows then. The link between the NAO and other teleconnection patterns and reverse-shear conditions in the Nordic Seas should be explored further. Overall, the Sea of Okhotsk follows a much more defined annual cycle, with the peak of polar low potential occurring in mid-December.

7. Acknowledgments

The author wishes to thank David Stephenson, Tom Bracegirdle, Ivar Seierstad, Nils Gunnar Kvamstø and one anonymous reviewer for reading the manuscript and providing many useful comments. This is publication Nr A 110 from the Bjerknes Centre for Climate Research.

References

Bluestein, H. B. 1992a. *Synoptic-Dynamic Meteorology in Midlatitudes. Volume I: Principles of Kinematics and Dynamics*, Oxford University Press.

Bluestein, H. B. 1992b. *Synoptic-Dynamic Meteorology in Midlatitudes. Volume II: Observations and Theory of Weather Systems*, Oxford University Press.

Bond, N. A. and Shapiro, M. A. 1991. Polar Lows over the Gulf of Alaska in Conditions of Reverse Shear. *Mon. Wea. Rev.* **119**, 551–572.

Businger, S. and Reed, R. J. 1989. Polar Lows. In *Polar and Arctic Lows*, (ed.P. F. Twitchell, E. Rasmussen and K. L. Davidson, A Deepak, Hampton, Virginia.

Claud, C., Heinemann, G., Raustein, E. and McMurdie, L. 2004. Polar low le cygne: Satellite observations and numerical simulations. *Quart. J. R. Meteorol. Soc.* **130**, 1075–1102.

Duncan, C. N. 1977. A numerical investigation of polar lows. *Quart. J. R. Meteorol. Soc.* **103**, 255–267.

Duncan, C. N. 1978. Baroclinic instability in a reversed shear flow. *Meteorological Magazine* **107**, 17–23.

Fu, G., Niino, H., Kimura, R. and Kato, T. 2004. A polar low over the Japan Sea on 21 january 1997. part I: Observational analysis. *Mon. Wea. Rev.* **132**, 1537–1551.

Grønås, S., Foss, A. and Lystad, M. 1987. Numerical simulations of polar lows in the Norwegian Sea. *Tellus* **39A**, 334–353.

Grønås, S. and Kvamstø, N. G. 1995. Numerical simulations of the synoptic conditions and development of arctic outbreak polar lows. *Tellus* **47A**, 797–814.

Harold, J. M., Bigg, G. R. and Turner, J. 1999. Mesocyclone activity over the Northeast Atlantic. part 2: An investigation of causal mechanisms. *International journal of climatology* **19**(12), 1283–1299.

Holton, J. R. 2004. *An Introduction to Dynamic Meteorology*, Elsevier Academic Press.

Kvingedal, B. 2004. Sea ice extent and variability in the nordic seas, 1967-2002, *AGU Monograph*, 200–210.

Liu, A. Q., Moore, G. W. K., Tsuboki, K. and Renfrew, I. A. 2004. A high-resolution simulation of convective roll clouds during a cold-air outbreak. *Geophys. Res. Lett.* **31**(3).

Lystad, M. 1986. *Polar Lows in the Norwegian Greenland and Barents Sea - Final report*, The Norwegian Meteorological Institute, Oslo.

Mailhot, J., Hanley, D., Bilodeau, B. and Hertzman, O. 1996. A numerical case study of a polar low in the Labrador Sea. *Tellus* **48A**, 383–402.

Montgomery, M. T. and Farrell, B. F. 1992. Polar low dynamics. *J. Atmos. Sci.* **49**, 2484–2505.

Noer, G. and Ovhed, M. 2003. Forecasting of Polar Lows in the Norwegian and the Barents Sea. *Proc. of the 9th meeting of the EGS Polar Lows Working Group*, Cambridge, UK.

Nordeng, T. E. and Rasmussen, E. A. 1992. A most beautiful polar low - a case study of a polar low development in the Bear Island region. *Tellus* **44A**, 81–99.

Orvik, K. A. and Niiler, P. 2002. Major pathways of Atlantic water in the northern North Atlantic and Nordic Seas toward Arctic. *Geophys. Res. Lett.* **29**(19), 1896–1899.

Rasmussen, E. A., Pedersen, T. S., Pedersen, L. T. and Turner, J. 1992. Polar lows and arctic instability lows in the Bear Island region. *Tellus* **44A**, 133–154.

Rasmussen, E. A. and Turner, J. 2003. *Polar lows*, Cambridge University Press.

Reed, R. J. and Duncan, C. N. 1987. Baroclinic instability as a mechanism for the serial development of polar lows: a case study. *Tellus* **39A**, 376–385.

Rogers, J. C. 1997. North Atlantic storm track variability and its association to the North Atlantic Oscillation and climate variability of Northern Europe. *J. Clim.* **10**(7), 1635–1647.

Wilhelmsen, K. 1985. Climatological study of gale-producing polar lows near Norway. *Tellus* **37A**, 451–459.

Wu, B., Wang, J. and Walsh, J. 2004. Possible Feedback of Winter Sea Ice in the Greenland and Barents Seas on the Local Atmosphere. *Mon. Wea. Rev.* **132**, 1868–1876.

Yanase, W., Niino, H. and Saito, K. 2002. High-resolution numerical simulation of a polar low. *Geophys. Res. Lett.* **29**(14), 1658–1661.